INDIAN JOURNAL OF SCIENCE AND TECHNOLOGY

RESEARCH ARTICLE

Investigation of Physical, Structural and Optical Properties of Borate Glasses with Chromium Doping for Optical Device Applications

Ravikumara Nayaka[1,2], Shrikant Biradar[1], Ashok Dinkar[1], Basavaraj Gurav[3], G B Devidas[1]*

1 Department of Physics, Kuvempu University, Shankaraghatta, Shimoga, 577 451, India
2 Department of Physics, Government First Grade College, Sangolli, Ranebennur, 577 451, Karnataka, India
3 Sangolli Rayanna First Grade College, Belagavi, 590017, Karnataka, India

OPEN ACCESS

Received: 13-11-2024
Accepted: 23-12-2024
Published: 31-01-2025

Citation: Nayaka R, Biradar S, Dinkar A, Gurav B, Devidas GB (2025) Investigation of Physical, Structural and Optical Properties of Borate Glasses with Chromium Doping for Optical Device Applications. Indian Journal of Science and Technology 18(2): 136-146. https://doi.org/10.17485/IJST/v18i2.3702

* **Corresponding author**.

devidasgb02@gmail.com

Funding: None

Competing Interests: None

Published By Indian Society for Education and Environment (iSee)

ISSN
Print: 0974-6846
Electronic: 0974-5645

Abstract

Objectives: The glass system with the composition (60-x)B_2O_3-1V_2O_5-19K_2O-10CaO-10BaO-xCr_2O_3 (where x = 0 to 1.0 mol %) was synthesized to explore physical, structural and optical characteristics of Cr-doped glasses. **Methods:** The glasses were fabricated using a conventional melt-quenching procedure at 1100ºC. The non-crystalline structure of the developed glasses was verified using X-ray diffraction analysis. The density of the glasses was determined using the Archimedes principle, and based on the density, other physical parameters were computed. The structural characteristics were examined using FTIR spectroscopy, while the optical properties were analyzed via UV-Visible spectroscopy. Additionally, photoluminescence spectra were investigated. **Findings:** XRD analysis verified the non-amorphous nature of the synthesized glasses. A rise in density from 2.532 to 5.705 g/cm^3 and a reduction in molar volume from 32.613 to 30.747 cm^3/mol of the glass samples were noted with increasing Cr_2O_3 content. FTIR analysis confirmed the presence of different structural groups such as BO_3, BO_4, Cr^{3+}, etc., and changes within the glass matrix. Optical absorption spectra show two absorption bands at 371 nm and 615 nm are attributed to $^4A_{2g} \rightarrow {}^4T_{1g}$ (F) and $^4A_{2g} \rightarrow {}^4T_{2g}$ electronic transitions. The optical band gap energy decreases from 3.556 to 2.998 eV showing structural changes and the formation of non-bridging oxygens and an increase in electron confinement. Additional optical parameters, including the refractive index, molar refraction, and metallization ratio, were assessed. Photoluminescence intensity increases as the content of the dopant increases in the glasses. **Novelty:** This study incorporated a combination of alkali elements and transition metal oxides in its formulation, which enhanced the structural and optical characteristics. The resulting optical data indicate that the synthesized glasses are well-suited for a range of optoelectronic device applications.

Keywords: Borate glasses; Chromium oxide; FTIR; Optical properties; Photoluminescence

1 Introduction

In recent years, glass materials have become more attractive and interesting in the field of science and engineering. Because, these are highly transparency, excellent metal ion solubility, easily synthesized, and ability to be easily shaped and modified, additionally these materials exhibit good stability [1,2]. Traditionally, glasses have been widely utilized in numerous areas, such as display technologies, soldering, scintillators, shielding, and optical amplifiers [2–4]. Especially, borate glasses have more potential characteristics such as low melting temperature, low optical basicity, good radiation protection, relatively elevated thermal expansion coefficients, high electrical conductivities and transparency spanning from the deep ultraviolet to the near infrared (185 nm to 3μm), high refractive index, mechanical and chemical stabilities [5,6].

Borate glasses infused with 3d transition metal ions have gained popularity in cutting-edge technological applications, including electronic and optoelectronic devices [1,7]. Many transitional metal oxides are there such as CoO, Fe_2O_3, ZnO, NiO, Cr_2O_3 etc., exhibit potential characteristics due to their various valence states of transition metal oxides. Among these, the chromium (Cr) cation is considered the best because the incorporation of Cr dopants in glasses influences both their color and physical properties. Cr, with an atomic number of 24 and an atomic weight of 51.996 g/mol, exhibits an electron configuration of $3d^5\ 4s^1$, rendering it a paramagnetic transition ion [1]. Among the various oxidation states of Cr, including Cr^{3+}, Cr^{4+}, Cr^{5+}, and Cr^{6+}, the most stable states are typically Cr^{3+} and Cr^{6+} ions. In glass systems, the introduction of Cr^{3+} and Cr^{6+} ions imparts distinct colors, which can be characterized through UV-VIS spectroscopy. Interestingly, Cr^{3+} is a highly stable dopant frequently utilized in various glass systems. Extensive research has been conducted on glass systems containing Cr cations [1,7,8].

BaO-containing glasses are highly significant due to their diverse applications, such as their suitability for liquid waste containment, use as a gamma-ray shielding materials, barrier in plasma display ribs, and crown optical lenses [9]. The incorporation of K_2O is anticipated to reduce the crystallization tendency of the glasses, improving mechanical durability and lowering the hygroscopic nature of the borate glass matrix [10]. Conversely, Calcium Oxide (CaO) acts as an effective network modifier, as borate creates open structural units with non-bridging oxygen ions in the glass structure upon the introduction of CaO into the glasses [11]. Vanadium is a robust transition metal commonly chosen for various applications, including solar cells, optoelectronics, and radiation shielding, due to its unpaired electron and multiple oxidation states (V^{3+}, V^{4+}, and V^{5+}) within the glass matrix [12].

Recently, there has been a growing interest in the development of glass materials infused with chromium ions for various applications. For example, Othman et al. [13] examined the impact of diverse bication additions on the optical properties of borate glasses composed of Li_2O-Cr_2O_3-B_2O_3-Bi_3O_3. They employed electron spin resonance (ESR) and photoluminescence spectroscopy to confirm the presence of Cr^{6+} and Cr^{3+} ions. N. Singkiburin et al. [14] described the physical, optical, and photoluminescent characteristics of Cr_2O_3 in borosilicate glasses, discovering increased reflection loss (R_L), reduced oxide polarizability, and decreased molar refractivity for 0.02 mol% of Cr_2O_3. Debjit Dutta et al. [15] presented a review article discussing the optical behavior of various chromium species within suitable glass matrices, summarized in the context of the host's chemical composition. These previous studies they primarily focused on the impact of 3d-transition metal ions, particularly Cr, on the structural and optical characteristics of glass hosts. However, there remains a

lack of research interest in exploring the incorporation of Cr into the glass matrix. The present study explores the physical and optical characteristics of Cr^{3+} ions incorporated into a Borate-Vanadium-potassium-Calcium-Barium glass matrix. We examined the concentration-dependent variations in both direct and indirect band gaps. Through a systematic evaluation of (60-x) B_2O_3-$1V_2O_5$-$19K_2O$-10CaO-10BaO-x Cr_2O_3 glasses, where x ranges from 0.2 to 1.0 mol%, we optimized the physical, structural and optical properties concerning Cr^{3+} concentration. This exploration aims to elucidate the suitability of these glasses for applications in near-infrared emitting solid-state devices.

2 Methodology

2.1 Preparation of glasses

The glass system, (60-x)B_2O_3-$1V_2O_5$-$19K_2O$-10CaO-10BaO-xCr_2O_3 with x values of 0.2, 0.4, 0.6, 0.8, and 1.0, corresponding to codes A0, A1, A2, A3, A4, and A5, was prepared using the conventional melt quenching technique. High-purity chemicals, including B_2O_3, V_2O_5, K_2CO_3, $CaCO_3$, $BaCO_3$, and Cr_2O_3 (all are of 99.8% purity and are purchased from LOBA Chemi. Ltd), were finely ground using an agate mortar to create a homogeneous powder. Each batch of the glass formula, weighing 15 gm (weighing balance with accuracy of 0.001g), was thoroughly mixed and placed in a porcelain crucible. The mixture was heated at 1100°C for 1 hour, and the resulting homogeneous melt was rapidly transferred to a pre-heated stainless brass plate and quenched to form uniform thick glass samples. To alleviate thermal stress, the glass underwent an annealing at 350°C for 3 hours before gradually cooling to ambient temperature. Figure 1 depicts the picture of the produced glasses while Table 1 shows the glass code and corresponding glass composition.

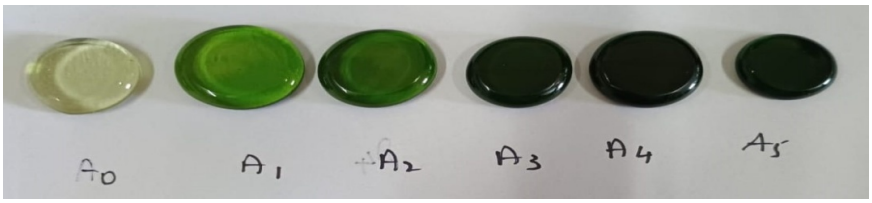

Fig 1. Picture of the fabricated glass samples

Table 1. Glass samples Code with different Cr_2O_3 compositions

Samples	Glass composition (mol %)
A0	60B_2O_3-$1V_2O_5$-$19K_2O$-10CaO-10BaO-0.0Cr_2O_3
A1	59.8B_2O_3-$1V_2O_5$-$19K_2O$-10CaO-10BaO-0.2Cr_2O_3
A2	59.6B_2O_3-$1V_2O_5$-$19K_2O$-10CaO-10BaO-0.4Cr_2O_3
A3	59.4B_2O_3-$1V_2O_5$-$19K_2O$-10CaO-10BaO-0.6Cr_2O_3
A4	59.2B_2O_3-$1V_2O_5$-$19K_2O$-10CaO-10BaO-0.8Cr_2O_3
A5	59B_2O_3-$1V_2O_5$-$19K_2O$-10CaO-10BaO-1.0Cr_2O_3

2.2 X-ray diffraction and physical properties

The powdered approach was employed to obtain the X-ray diffraction pattern of the glass samples. CuKα with a wavelength of 1.5402 nm served as the source in the diffractometer by utilizing the Rigaku Miniflex 600 and which having sensitivity of 2°/minute. The density of the glasses were evaluated using Archimedes principle using a digital balance (with accuracy of 0.001g) and toluene is used as an immersion liquid with a density of 0.866 g/cm^3. The density was computed utilizing the following formula[16]:

$$\rho = \frac{W_a}{W_a\text{-}W_L} \times \rho_L \quad (1)$$

where W_a refers to the glass's weight when measured in air, W_L represents its weight when submerged in a liquid. And ρ_L refers to the immersion liquid's density. Via the following equation, the produced glasses ρ and M (molecular weight of glass) can be used to calculate the molar volume (V_M)[17]:

$$V_M = \frac{M}{\rho} \tag{2}$$

Meanwhile, the following expressions (Equations (3), (4), (5) and (6)) have been used to determine the concentration of the ion (N), radius of polaron (r_p), inter-ion distances (r_i), and field strength (F_S)[17,18]:

$$N = \frac{mol\%\ x\ \rho\ x\ N_A}{M_w} \tag{3}$$

$$r_p = \left(\frac{1}{2}\right)\left(\frac{\pi}{6N}\right)^{1/3} \tag{4}$$

$$r_i = \left(\frac{1}{N}\right)^{1/3} \tag{5}$$

$$F_s = \frac{Z}{r_p^2} \tag{6}$$

where N_A refers to Avogadro's number, M is the mean molecular weight, mol% defines the chromium ratio, and Z is the Cr atomic number.

2.3 Fourier transform infrared (FTIR), UV-Visible and Photoluminescence studies

FTIR spectra were recorded at room temperature using a Perkin Elmer Lambda PRONTIER (MIV-FTIR) spectrophotometer. The glass samples acquired were shaped for characterization. Optical absorption spectra of the present glass were measured in the UV/VIS/NIR region of 190-1100 nm (with sensitivity of $\pm$5 nm) using a Perkin Elmer Lambda 950 UV/VIS/NIR spectrophotometer.

By utilizing absorption, the indirect energy band gap (E_g) of the samples can be computed by employing the Mott and Devis formula[19]:

$$\alpha h\nu = C\left(h\nu - E_g\right)^2 \tag{7}$$

where C is constant, E_g refers to the energy band gap, and hν represents the photon energy. α is the coefficient of absorption, it is computed by using the expression[19]:

$$\alpha = \frac{2.303\ x\ \ A}{t} \tag{8}$$

where A defines the absorbance and t indicates the glass thickness.

The refractive index (n) related to the local field and electronic polarization of ions in the materials is one of the most essential optically dependent sample features. The following formula can be employed to assess the refractive index (n)[20].

$$\frac{(n^2-1)}{(n^2+2)} = 1 - \sqrt{\frac{E_g}{20}} \tag{9}$$

The dielectric constant (ε) is computed using the n value as follows.

$$\varepsilon = n^2 \tag{10}$$

The reflection loss (R_L) on the glass plane is evaluated using the relation [20]:

$$R_L = \left(\frac{n-1}{n+2}\right)^2 \tag{11}$$

Molar refractivity (R_M) can be computed using the following formula [20,21]:

$$R_M = \left(\frac{n^2-1}{n^2+2}\right) V_M \tag{12}$$

Optical transmission (T) can be determined by using the below expression

$$T = \frac{2n}{n^2+1} \tag{13}$$

The metallization criterion (M) predicts whether a material will behave as a metal or an insulator and is computed using the following relation [22].

$$M = 1 - \frac{R_M}{V_M} \tag{14}$$

Photoluminescence spectra were recorded using near-infrared spectrophotometers (Quanta Master (QM)-300, PTI-Horiba) with Xenon as the source.

3 Results and discussion

3.1 X-ray diffraction (XRD) analysis

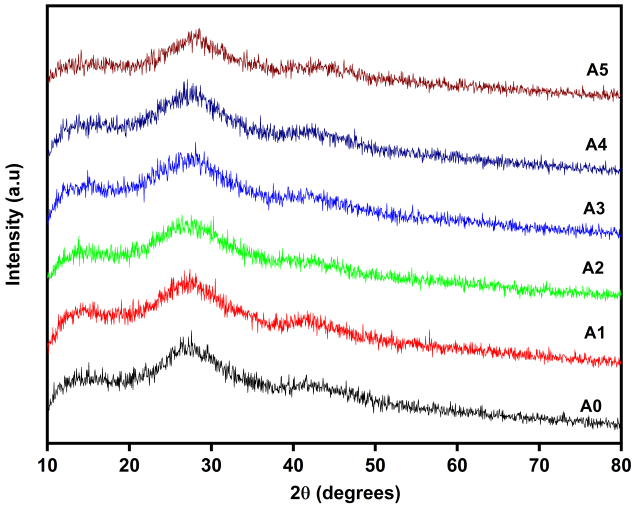

Fig 2. XRD spectra of synthesized glasses

The confirmation of the amorphous characteristics of the synthesized glass system is examined by the X-ray diffraction (XRD) in the range of 10-80° illustrated in Figure 2, the spectra clearly reveal, across all Cr doped glass matrix each pattern exhibits a broad and diffuse scattering at lower angles (around 20-30°), and the lack of distinct diffraction peaks suggests the presence of structural irregularities within the generated glass matrix. This observation serves to confirm the amorphous nature of the synthesized glass samples [23].

3.2. Physical properties

The physical parameters of the prepared glasses were calculated using Equations (1), (2), (3), (4), (5) and (6), and their values are presented in Table 2. Density (ρ) is an important parameter that describes the compactness and structural changes in materials. The variation of density (ρ) and molar volume (V_M) with Cr_2O_3 loading is depicted in Figure 3. Notably, as the Cr_2O_3 content increased, the density of the glasses grew from 2.532 to 2.572 g/cm^3, while the molar volume reduced from 31.693 to 30.747 cm^3/mol. The rise in ρ is linked to the replacement of the lighter B_2O_3 (molar mass 69.62 g/mol) with the heavier Cr_2O_3 (molar mass 151.99 g/mol)[24]. As the concentration of Cr_2O_3 increases, V_M decreases, suggesting greater compactness in the glass structure[13,24]. This effect, often referred to as network shrinkage, occurs because Cr_2O_3 fills interstitial spaces within the network, leading to a more tightly packed arrangement. Other physical parameters were evaluated, including ion concentration (N), inter-nuclear distance (r_i), polaron radius (r_p), and field strength (F_s). The findings indicate that increasing Cr_2O_3 content results in an elevation of N and F_s. Additionally, the decrease in r_i and r_p indicates a transition toward a more densely packed glass structure, which can be attributed to the network-modifying role of chromium ions[13,25].

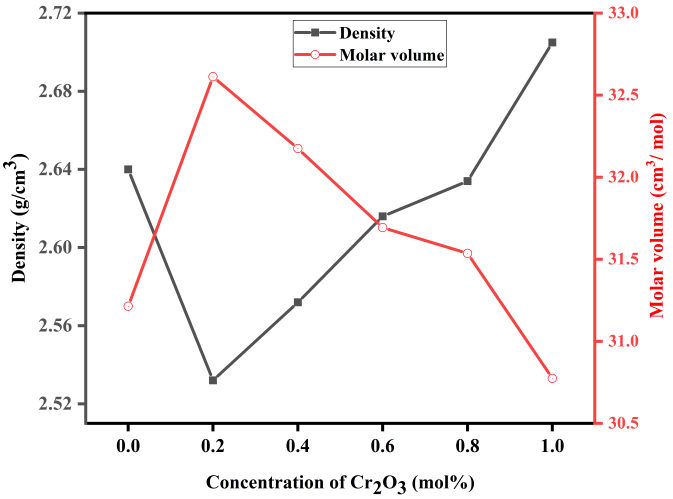

Fig 3. Variation of density and molar volume with Cr_2O_3 content

Table 2. Physical parameters of Cr_2O_3 doped glasses

Physical parameters	Glass samples					
	A0	A1	A2	A3	A4	A5
Density (gm/cm^3)	2.640	2.532	2.572	2.616	2.634	2.705
Molar volume (cm^3/ mol)	31.214	32.613	32.175	31.693	31.536	30.747
Ion concentration (Nx10^{23} ion/cm^3)	-	0.308	0.295	0.299	0.304	0.305
Polaron radius, $\left(r_p \times \mathring{A}\right)$	-	1.307	1.327	1.320	1.314	1.312
Inter-nuclear distance, $\left(r_i \times \mathring{A}\right)$	-	3.243	3.291	3.276	3.260	3.254
Field strength, (F_s x 10^{17} cm^{-1})	-	3.743	3.635	3.669	3.706	3.718

3.3 FTIR analysis

Fourier-transform infrared (FT-IR) spectroscopy is an effective method for the identification and analysis of structural units of developed glass networks. Also, the analysis of IR spectra can unveil details about the rotation and vibration of various molecules embedded within a glass matrix. These vibrations, characterized by their frequencies, distinguish themselves from

those of other molecular groups in the matrix, each possessing a unique vibrational frequency characteristic.Figure 4 illustrates the FTIR spectra of A0 to A5 glass samples measured in the wave number range of 400 to 4000 cm^{-1}. All the bands detected in the range of 2000 to 4000 cm^{-1} are due to vibrations associated with OH groups, H-O-H bonds, and hydrogen bonds. There are three primary active regions of FTIR spectra for the borate glass system. They are: (i) approximately 600-800 cm^{-1}, related to the bending modes from various types of borate units; (ii) around 800-1200 cm^{-1}, associated with the stretching vibrations of B-O bonds in BO_4 units; and (iii) around 1200-1600 cm^{-1}, linked to the stretching vibrations of B-O bonds connected with BO_3 units[5,17].

The peak detected at 556 cm^{-1} is ascribed to the presence of Ca^{2+} ions. The peak appearing at 710 cm^{-1} is associated with the bending vibrations of B–O–B, and its intensity diminishes as the Cr concentration rises. The peak centered at 994 cm^{-1} is related to the B–O stretching vibrations within BO_4 tetrahedra, which are commonly found in diborate configurations[16,17]. Furthermore, the peak located at 1394 cm^{-1} signifies the asymmetric stretching vibrations of B–O bonds within trigonal BO_3 groups, typically present in metaborate, pyroborate, and orthoborate arrangements[17,20]. The bands detected above 1600 cm^{-1} arise from the stretching and bending vibrations of water molecules. The IR response within the spectral regions corresponding to BO_4 and BO_3 undergoes significant changes as the chromium concentration increases[17,20]. Specifically, the intensity of two broad IR bands, observed between 800 and 1200 cm^{-1} (linked to BO_4 groups) and 1200-1600 cm^{-1} (associated with BO_3 groups), diminishes with the rise in chromium content. This implies that chromium acts as a network modifier as it integrates into the structural network and causes the formation of non-bridging oxygens (NBOs) in the glass structure.

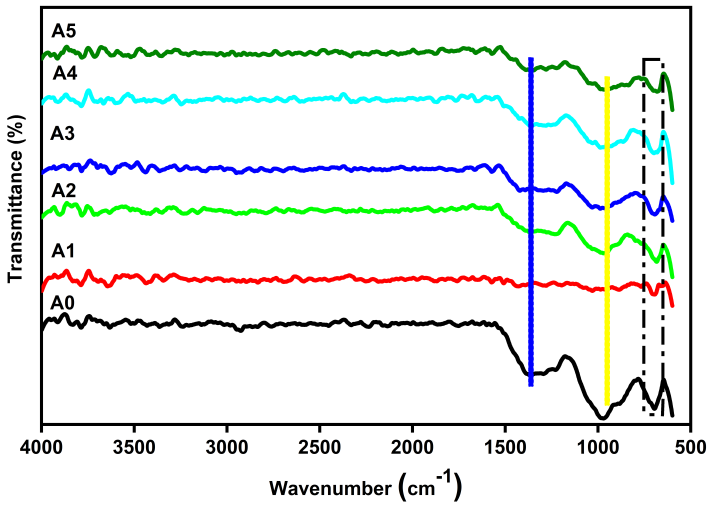

Fig 4. FTIR spectra of synthesized glass samples

3.4 UV-Vis absorption spectra

For the produced glasses, the optical absorbance (A) spectra were recorded in the wavelength range of 200–1100 nm, as depicted in Figure 5. It was noticed in the spectra that two absorption peaks at 371 nm and 615 nm were generated with the incorporation of Cr_2O_3. Moreover, the intensity and width of these two bands increase with higher Cr_2O_3 concentrations. It is well-established that the incorporation of Cr^{3+} into the glass compositions imparts a green hue to the glasses, which arises from the absorption bands in the visible spectrum. For the fabricated glasses, along with the absorption spectra, we can observe from Figure 1 the color change from pale green to deep green with the addition of Cr_2O_3. The two absorption bands at 371 nm and 615 nm are attributed to $^4A_{2g} \rightarrow {}^4T_{1g}$ (F) and $^4A_{2g} \rightarrow {}^4T_{2g}$ electronic transitions[26,27].

The Tauc plot in Figure 6 illustrates indirect transitions, with the indirect band gap energy (E_g) gradually decreasing from 3.702 to 2.988 eV as the Cr_2O_3 concentration increases. This reduction in E_g is likely due to structural modifications resulting from the addition of Cr_3O_3. The incorporation of Cr_2O_3 may enhance electron localization, increasing the number of donor centers within the glass matrix. Consequently, the E_g of the glasses decreases as the Cr_2O_3 content rises[26,28].

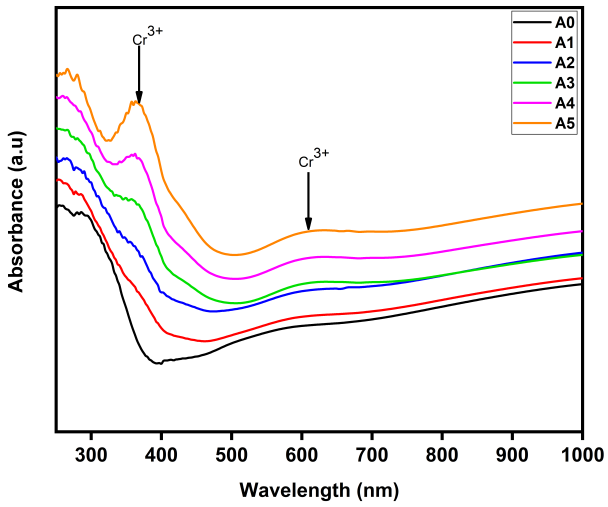

Fig 5. Absorption spectra of synthesized glass samples

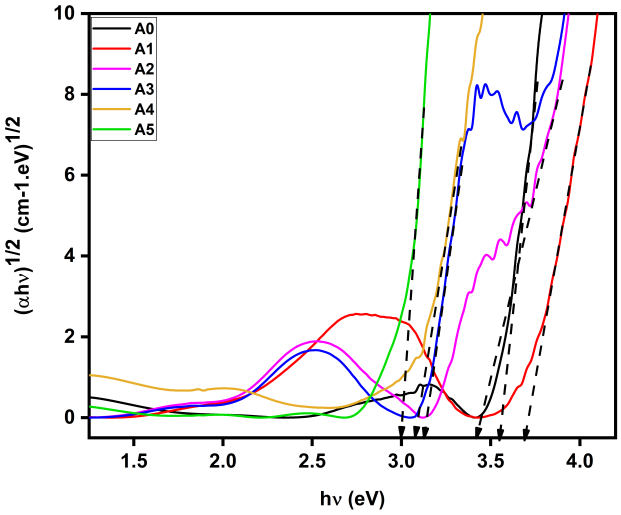

Fig 6. Variation of $(\alpha h\nu)^{1/2}$ with $h\nu$ for the synthesized glasses

Table 3. Optical properties of the synthesized A-series glasses

Optical properties	Glass samples					
	A0	A1	A2	A3	A4	A5
Energy band gap, E_g (eV)	3.556	3.702	3.401	3.116	3.083	2.988
Refractive index, n	2.261	2.230	2.296	2.366	2.375	2.400
Dielectric constant, ε	5.114	4.972	5.274	5.600	5.640	5.761
Molar refraction, R_M (cm^3/mol)	18.057	18.586	18.908	19.186	19.259	19.381
Reflection loss, R_L	0.578	0.569	0.587	0.605	0.607	0.613
Metallization criteria, M	0.421	0.430	0.412	0.394	0.392	0.386
Optical transmission, T	0.739	0.736	0.732	0.717	0.715	0.709

Another significant parameter, the refractive index (n), was determined using the Dimitrov-Sakka relation given by Equation (9), and the values are presented in Table 3. The findings show that n increases from 2.230 to 2.400 as the Cr_2O_3 loading grows. This increase is attributed to the enhanced compactness of the glass network structure, as reflected by the corresponding rise in glass density[20,27]. Additionally, the values of dielectric constant (ε), reflection loss (R_L), and molar refractivity (R_M) were computed using Equations (10), (11) and (12), respectively. These parameters increased with higher Cr_2O_3 content, due to the rise in n values, indicating a more densely packed structure in the prepared glasses. Furthermore, transmission (computed by using Equation (13)) declines from 0.739 to 0.709 as the Cr_2O_3 content rises in the glass matrix[17,20]. The metallization criterion (M) was applied to predict whether the material exhibits metallic or non-metallic behavior and it was calculated using Equation (14). The corresponding values are displayed in Table 3. The calculated M values are less than one and show a downward trend, confirming that the prepared glasses demonstrate a decreasing non-metallic nature[21].

3.5 Emission spectra

Emission spectra of the Cr doped glass matrix (A0 to A5) are presented in Figure 7. This image exhibits distinct variation in the intensity and position of emission peaks, these emissions are due to the influence of different Cr doping levels and glass compositions on their luminescent properties. The emission spectra for all samples display peaks in the range of 600 to 1100 nm, with the most prominent peak observed around 660 nm. The intensity and position of these emission peaks vary among the samples, indicating the different effects of Cr doping levels. Sample A3 shows the highest intensity emission peak around 670 nm, suggesting a strong luminescence likely due to optimal Cr doping levels. This high-intensity emission makes sample A3 potentially suitable for applications requiring strong luminescence, such as in lighting and displays. On the other hand, sample A2, exhibits a distinct lower intensity peak around 670 nm, indicating that the Cr level affects its luminescent properties. Similarly, samples A0, A1, A4, and A5 also show significant emission intensities. In addition to the sharp peak around 670 nm, broad emission bands are observed in the 900-1500 nm range for all samples. These broader bands indicate complex luminescent behavior influenced by Cr in the glass matrix composition[29,30]. The differences in peak intensities and positions among the samples suggest that varying the Cr doping levels; results in distinct emission characteristics[13,30].

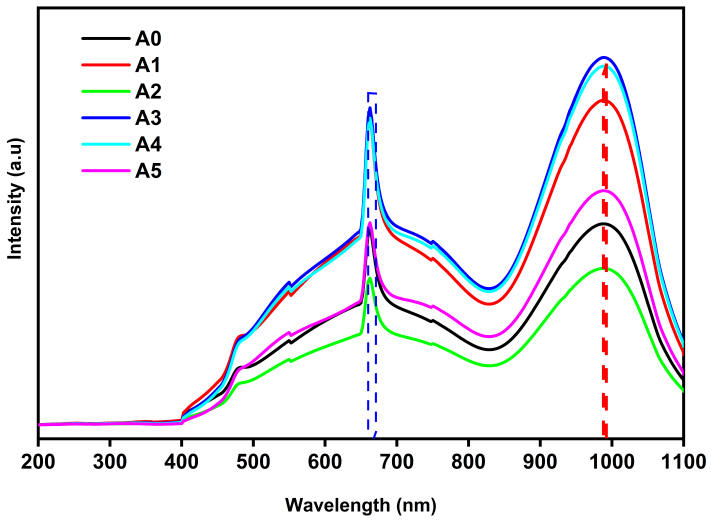

Fig 7. Emission spectra of synthesized glass samples

3.6 Photoluminescence study

The photoluminescence (PL) emission spectra of the current glass system, depicted in Fig. 9 and excited at a wavelength of 350 nm, reveal distinct features in the near-infrared (NIR) region spanning from 450 to 550 nm. Notably, two prominent bands emerge around ~495 nm and ~650 nm, indicating strong emissions. While these bands are primarily attributed to the presence of Cr^{3+} ions, it's noteworthy that the luminescence intensity exhibits a gradual increase with the incorporation of Cr_2O_3.

Moreover, the luminescence signals are further enhanced by the successive reduction of B^{3+} ions in the samples. Interestingly, a similar improvement in luminescence intensity is observed with the addition of Cr^{3+} ions, as illustrated in Figure 8. The emission bands spanning from 600 to 800 nm are attributed to the luminous transitions of Cr^{3+} ions positioned tetrahedral. These transitions correspond to the excited states 2E(2G) and 4 T1(4P). Notably, in the current system, emissions from the metastable state 2E (2 G) are not observed. Instead, the identified emission bands stem from the 4 T1 (4P) excited state. Specifically, bands around ~765 nm, ~790 nm, and ~850 nm can be linked to transitions $^4T_1(^4P) \rightarrow 4\ A_2(^4F)$, $^4T_1(^4P) \rightarrow {}^4T_2(4F)$, and $^4T_1(^4P) \rightarrow {}^4T_1(^4F)$, respectively[13,29].

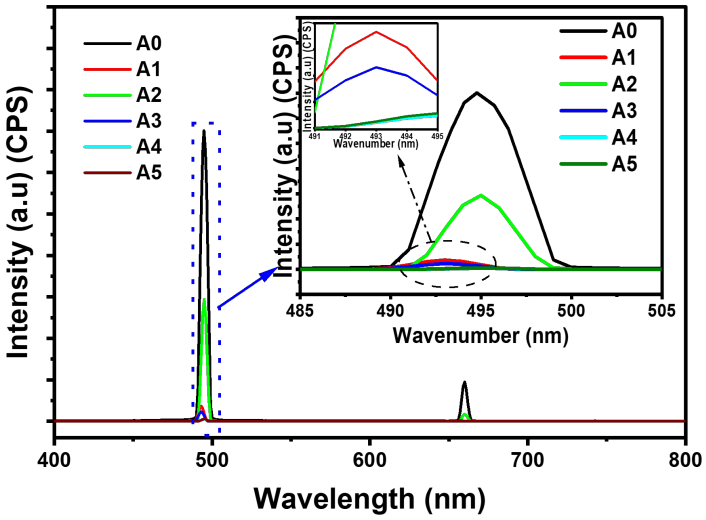

Fig 8. Photoluminescence spectra of synthesized glass samples

4 Conclusion

In this study, the (60-x)B_2O_3-1V_2O_5-19K_2O-10CaO-10BaO-xCr_2O_3 glass system (x = 0.2 to 1.0) exhibited notable structural, optical, and physical changes as Cr_2O_3 content increased. XRD analysis confirmed the amorphous nature of the samples, and the density of the glasses increased from 2.532 to 2.705 g/cm^3 with rising Cr_2O_3 content. FTIR spectroscopy highlighted key vibrational modes associated with BO_3, $Cr^{3+,}$ and BO_4 units, with noticeable shifts and intensity changes due to Cr incorporation. Optical absorption revealed peaks at 371 nm and 615 nm, linked to Cr^{3+} transitions, resulting in a green hue. Increasing Cr_2O_3 reduced the band gap energy (E_g) from 3.556 to 2.998 eV, indicating structural alterations, an increase in donor centers, and a rise in the refractive index (n) from 2.261 to 2.400, suggesting enhanced structural compactness. An increase in the dielectric constant, molar refraction, and reflection loss, along with a decrease in metallization values, indicates that the prepared glasses exhibit enhanced optical characteristics. Additionally, emission spectra showed strong luminescence, particularly in sample A3, making it suitable for lighting applications. These findings underscore the role of Cr_2O_3 as a network modifier, improving both the optical and structural properties of the glass, with potential uses in optoelectronics.

References

1) Sadeq MS, Elashry MY, El-Daly AA, Ibrahim AH. Environmental influence of high Na2O additions on microstructure and ligand field parameters of Cr3+ inside borosilicate glass. *Ceramics International*. 2023;49(16):27201– 27213. Available from: https://doi.org/10.1016/j.ceramint.2023.05.268.
2) Sayyed MI, Biradar S, Hanafy TA, Maghrbi Y, Faruque MR, Abdullah S, et al. Optimization of optical properties and radiation shielding efficiency in BaO-PbO2-B2O3-Dy2O3 glass systems. *Optical Materials*. 2024;157. Available from: https://doi.org/10.1016/j.optmat.2024.116205.
3) Shaaban KS, Al-Baradi AM, Ali AM. Cr2O3 effect on the structure, optical, and radiation shielding properties of Na2B4O7-SiO2-CaO-Cr2O3 glasses. *Applied Physics A*. 2022;128. Available from: https://link.springer.com/article/10.1007/s00339-022-05348-9.
4) Biradar S, Dinkar A, Devidas GB. A Comprehensive Study of the Effect of BaO Doping on the Physical, Mechanical, Optical, and Radiation Shielding Properties of Borate-Based Glasses. *Nexus of Future Materials*. 2024;1(3). Available from: https://doi.org/10.70128/584259.
5) Byalollikar DG, Biradar S, Dinkar A, Sankarappa T, Biradar J. Impact of bismuth oxide on structural, optical and gamma-ray shielding properties of calcium-sodium-borate glasses. *Radiation Protection Dosimetry*. 2024;200(11-12):1207–1215. Available from: https://doi.org/10.1093/rpd/ncae066.

6) Devidas GB, Dinkar A, Biradar S. Effect of gamma irradiation on dielectric and ac conductivity studies of bismuth borate glasses doped with V2O5. *Indian Journal of Science and Technology*. 2023;16(8):598–604. Available from: https://doi.org/10.17485/IJST/v16i8.2305.
7) Sayyed MI, Abdo MA, Ali HE, Sadeq MS. Transparent and radiation shielding effective Na2O- CrO3 borate glasses via AgI additives. *Ceramics International*. 2022;48(20):30817–30825. Available from: https://doi.org/10.1016/j.ceramint.2022.07.035.
8) Morshidy HY, El-Fattah ZMA, Abul-Magd AA, Hassan MA, Mohamed AR. Reevaluation of Cr6+ optical transitions through Gd2O3 doping of chromium-borate glasses. *Optical Materials*. 2021;113. Available from: https://doi.org/10.1016/j.optmat.2021.110881.
9) Gomaa HM, Abu-Khadra AS, Algarni H, Yahia IS, Zahran HY, Abdel-Ghany AM. Effect of BaO doping on the structural and optical properties of some cerium-copper sodium borate glasses. *Journal of the Australian Ceramic Society*. 2023;59:343–353. Available from: https://link.springer.com/article/10.1007/s41779-023-00859-x#:~:text=Adding%20a%20few%20percent%20of,as%20special%20optical%20glassy%20materials.
10) Manjeet, Kumar A, Anu, Ravina, Deopa N, Kumar A, et al. Structural, thermal, optical and luminescence properties of Dy3+ ions doped Zinc Potassium Alumino Borate glasses for optoelectronics applications. *Journal of Non-Crystalline Solids*. 2022;588. Available from: https://doi.org/10.1016/j.jnoncrysol.2022.121613.
11) Ilik E, Kavaz E, Kilic G, Issa SA, Almisned G, Tekin HO. Synthesis and characterization of vanadium (V) oxide reinforced calcium-borate glasses: experimental assessments on Al2O3/BaO2/ZnO contributions. *Journal of Non-Crystalline Solids*. 2022;580. Available from: https://doi.org/10.1016/j.jnoncrysol.2022.121397.
12) Abdel-Karim AM, Fayad AM, El-Kashef IM, Saleh HA. Influence of vanadium oxide on the optical and electrical properties of Li (Oxide or Fluoride) borate glasses. *Journal of Electronic Materials*. 2023;52(4):2409–2420. Available from: https://link.springer.com/article/10.1007/s11664-022-10187-8.
13) Othman AM, El-Fattah ZMA, Farouk M, Moneep AM, and MAH. Optical spectroscopy of chromium doped bismuth-lithium borate glasses. *Journal of Non-Crystalline Solids*. 2021;558. Available from: https://doi.org/10.1016/j.jnoncrysol.2021.120665.
14) Singkiburin N, Mahingsa N, Srisittipokakun N, Luewarasirikul N, Rajaramakrishna R, Kothan S, et al. Physical, optical, and photoluminescence properties of Cr2O3 in borosilicate glasses. *Integrated Ferroelectrics*. 2023;238(1):343–355. Available from: https://doi.org/10.1080/10584587.2023.2234583.
15) Dutta D, Dhar A, Das S, Paul MC. Chromium Doped Glasses for Photonic Applications: A Brief Review and Prospects. *Transactions of the Indian Ceramic Society*. 2023;82(3):209–228. Available from: https://doi.org/10.1080/0371750X.2023.2227665.
16) Kaky KM, Sayyed MI, Hamad MK, Biradar S, Mhareb MH, Altimari U, et al. Bismuth oxide effects on optical, structural, mechanical, and radiation shielding features of borosilicate glasses. *Optical Materials*. 2024;155. Available from: https://doi.org/10.1016/j.optmat.2024.115853.
17) Biradar S, Dinkar A, Manjunatha, Bennal AS, Devidas GB, Hareesh BT, et al. Comprehensive investigation of borate-based glasses doped with BaO: an assessment of physical, structural, thermal, optical, and radiation shielding properties. *Optical Materials*. 2024;150. Available from: https://doi.org/10.1016/j.optmat.2024.115176.
18) Mastanappa A, Biradar S, Devidas GB, Rajaramakrishna R, Sayyed MI, Chandrashekara MN. Effect of Li2O on physical, structural, thermal, optical, and electrical properties of mixed alkali borate glasses containing silver nanoparticles. *Optical Materials*. 2024;157. Available from: https://doi.org/10.1016/j.optmat.2024.116224.
19) Sayyed MI, Zaiter MJ, Mhareb MHA, Mahmoud KA, Biradar S, Mahdi RI, et al. Optical, physical, mechanical, structural, and radiation shielding investigations of B2O3–TeO2-GeO2-MgO-PbO for ionizing protection and optical transmission application. *Optical Materials*. 2024;154. Available from: https://dx.doi.org/10.1016/j.optmat.2024.115807.
20) Biradar S, Chandrashekara MN, Dinkar A, Manjunatha, Devidas GB, Bennal AS, et al. A multifaceted study of B2O3-BaO-PbO-WO3 glasses doped with Bi2O3: Insights from physical, thermal, structural, mechanical and optical analyses towards improved shielding properties. *Ceramics International*. 2024;50(17):29332–29345. Available from: https://doi.org/10.1016/j.ceramint.2024.05.227.
21) Kaky KM, Sayyed MI, Mahmoud KA, Mhareb MH, Biradar S, Kadhim AJ. A comprehensive investigation on lanthanum ions doped borate-tellurite-germinate glass for radiation shielding and optical application. *Progress in Nuclear Energy*. 2024;176:105402–105402. Available from: https://doi.org/10.1016/j.pnucene.2024.105402.
22) Biradar S, Chandrashekara MN, Manjunatha, Dinkar A, Devidas GB, Bennal AS, et al. Synergistic optimization of physical, thermal, structural, mechanical, optical and radiation shielding characteristics in borate glasses doped with Bi2O3. *Optical Materials*. 2024;155. Available from: https://dx.doi.org/10.1016/j.optmat.2024.115815.
23) Gurav B, Devidas GB, Dinkar A, Biradar S, Rajaramakrishna R. Photoluminescence Interaction of Alkali Fluoride Over Alkali Oxide in Nd3+ Doped Glasses for NIR Applications. *Indian Journal Of Science And Technology*. 2023;16(3):230–238. Available from: https://indjst.org/articles/photoluminescence-interaction-of-alkali-fluoride-over-alkali-oxide-in-nd3-doped-glasses-for-nir-applications.
24) Maan D, Nain D, Meenakshi. Investigating Structure and Physical Properties of Chromium Oxide Doped Bismuth Borate Glasses. *Indian Journal of Pure & Applied Physics*. 2024;62(6):429–469. Available from: https://or.niscpr.res.in/index.php/IJPAP/article/view/8667.
25) Kashif I, Ratep A. Optical properties of borate glasses containing chromium and erbium oxide. *Applied Physics A*. 2023;129. Available from: https://dx.doi.org/10.1007/s00339-023-06764-1.
26) Al-Ghamdi H, Alsaif NAM, Khattari ZY, Shams MS, El-Refaey AM, Sadeq MS, et al. Exploring the physical, vibrational, optical, and dielectric properties of chromium-doped bismo-borate barium glasses for potential use in optical applications. *Optical and Quantum Electronics*. 2023;55. Available from: https://dx.doi.org/10.1007/s11082-023-05129-5.
27) Al-Buriahi MS, Alajerami YSM, Abouhaswa AS, Alalawi A, Nutaro T, Tonguc B. Effect of chromium oxide on the physical, optical, and radiation shielding properties of lead sodium borate glasses. *Journal of Non-Crystalline Solids*. 2020;544. Available from: https://dx.doi.org/10.1016/j.jnoncrysol.2020.120171.
28) Slibi DA, Hassan MA, El-Fattah ZMA, Atallah M, El-Sherbiny MA, Farouk M. Optical transitions from hexavalent chromium in lithium-borate glasses. *Optical and Quantum Electronics*. 2021;53. Available from: https://dx.doi.org/10.1007/s11082-021-03147-9.
29) Samdani, Ramadevudu G, Chary MN, Shareefuddin M. Physical and spectroscopic studies of Cr3+ doped mixed alkaline earth oxide borate glasses. *Materials Chemistry and Physics*. 2017;186:382–389. Available from: https://dx.doi.org/10.1016/j.matchemphys.2016.11.009.
30) Luewarasirikul N, Ruangthaweep Y, Kaewkhao J. Preparation and Spectroscopic Studies of Cr3+-doped Aluminium Calcium Sodium Borate Glasses. *Materials Today: Proceedings*. 2019;17:1831–1836. Available from: https://dx.doi.org/10.1016/j.matpr.2019.06.220.